Formation Mechanism and Composition Distribution of FePt Nanoparticles

G. B. Thompson – The University of Alabama
et al.

Citation of published version:

Srivastava, C., et al. (2007): Formation Mechanism and Composition Distribution of FePt Nanoparticles. *Journal of Applied Physics*, 102(10).
DOI: https://doi.org/10.1063/1.2816227

Formation mechanism and composition distribution of FePt nanoparticles

Chandan Srivastava
Department of Metallurgical and Materials Engineering, University of Alabama, Tuscaloosa, Alabama 35487, USA

Jayendra Balasubramanian
Department of Chemical and Biological Engineering, University of Alabama, Tuscaloosa, Alabama 35487, USA

C. Heath Turner and John M. Wiest
Department of Chemical and Biological Engineering, University of Alabama, Tuscaloosa, Alabama 35487, USA

Hitesh G. Bagaria
Department of Chemical and Biomolecular Engineering, Rice University, Houston, Texas, 77251, USA

Gregory B. Thompson[a)]
Department of Metallurgical and Materials Engineering, University of Alabama, Tuscaloosa, Alabama 35487, USA

(Received 16 July 2007; accepted 23 September 2007; published online 27 November 2007)

Self-assembled FePt nanoparticle arrays are candidate structures for ultrahigh density magnetic storage media. One of the factors limiting their application to this technology is particle-to-particle compositional variation. This variation will affect the $A1$ to $L1_0$ transformation as well as the magnetic properties of the nanoparticles. In the present study, an analysis is provided for the formation mechanism of these nanoparticles when synthesized by the superhydride reduction method. Additionally, a comparison is provided of the composition distributions of nanoparticles synthesized by the thermal decomposition of $Fe(CO)_5$ and the reduction of $FeCl_2$ by superhydride. The latter process produced a much narrower composition distribution. A thermodynamic analysis of the mechanism is described in terms of free energy perturbation Monte Carlo simulations.
 [DOI: 10.1063/1.2816227]

I. INTRODUCTION

Self-assembled FePt nanoparticle arrays are candidates for next generation magnetic storage media.[1] The size of these nanoparticles as well as their high packing fraction allows for the possibility of storage densities greater than 1 TB/in.[2] There are some fundamental issues that limit the application of this material in magnetic storage devices. Most wet chemistry synthetic procedures produce nanoparticles with a metastable, solid-solution face-centered-cubic (fcc) structure (the $A1$ structure) which can be superparamagnetic depending on the size of the particle.[2] A subsequent anneal transforms the particles from the $A1$ to the desired $L1_0$ structure, which has high magnetocrystalline anisotropy.[1] However, during annealing the particles agglomerate and sinter destroying the self-assembled arrays.[3] Additionally, for their use in perpendicular magnetic storage media, the particles in the film must have aligned magnetic easy axes.[4] There has been progress in resolving several of these issues. Ordered $L1_0$ FePt nanoparticles have been directly synthesized from solution[5] and $A1$ FePt nanoparticles can be annealed in a salt bath to a high degree of order without sintering.[6] Furthermore, Kang *et al.*[4] have reported promising work on easy-axis alignment by drying $L1_0$ nanoparticle dispersions in a magnetic field.

Despite these successes, there still remain key questions on particle-to-particle compositional variation. The magnetic properties of $L1_0$ FePt nanoparticles depend strongly on the composition and size of the particles.[7] The established wet chemical methods used to produce FePt nanoparticles[1,8,9] involve nucleation and growth in the reaction mixture. One of the factors that may affect the formation mechanism is the choice of metallic precursors for Fe and Pt. Differences in the metal source for synthesizing the nanoparticles can lead to a final reaction product with compositional variation between individual particles.

There are few reports in the literature that specifically correlate the average composition of a nanoparticle dispersion to the composition variability on a particle-to-particle basis.[10] The report in Ref. 10 shows that FePt nanoparticles synthesized by the method reported in Ref. 1, involving the reduction of $Pt(acac)_2$ and the thermal decomposition of $Fe(CO)_5$, has a particle-to-particle composition variation from 21 to 70 at. % Fe. Furthermore, only a fraction of the particles (29%) in the dispersion have the desired nearly equiatomic composition. It has been established that a nearly equiatomic composition (slightly Fe rich) is associated with maximum tetragonality and thus the highest magnetocrystalline anisotropy.[11] Studies of the transformation and magnetic properties take into account the average composition of the nanoparticle dispersion but rarely address the same issue on

[a)]Electronic mail: gthompson@eng.ua.edu

a single particle level. Moreover, these variations in individual particle composition will severely affect the ultimate quality of self-assembled arrays in a storage medium. Analysis of the reaction mechanism by the choice of metallic precursors is required to determine (1) if there are specific wet chemistry methods that minimize individual particle compositional variation and (2) the sequence of the nucleation and growth of the nanoparticles and how that contributes to the compositional variation.

In this paper the composition distribution study has been divided into two parts. In the first section, the composition distributions of FePt nanoparticles synthesized from two different procedures are compared. The second section addresses in detail the mechanism of formation of these nanoparticles by one of the methods, the superhydride synthesis,[8] which shows a smaller variation in the particle-to-particle composition. Monte Carlo simulation based free energy perturbation (FEP) calculations are used to rationalize the experimental observations.

II. EXPERIMENTAL PROCEDURES

To study the variation in composition distribution in FePt nanoparticles as a function of the synthetic procedure, particles were synthesized by the iron pentacarbonyl[1] and superhydride methods.[8] In the iron pentacarbonyl method, $Fe(CO)_5$ and $Pt(acac)_2$ were used as the sources for Fe and Pt, respectively. The required amount of Pt salt (0.5 mmol) was placed in a three neck round bottom flask along with 0.52 g of 1, 2 hexadecanediol, (a reducing agent), and 25 ml of diphenyl ether solvent. The flask was equipped with a magnetic stirrer, a reflux condenser, a thermometer, and a rubber septum. The reaction was performed under a nitrogen atmosphere and the reaction mixture was heated to 100 °C, at which temperature 0.5 mmol of oleic acid, 0.5 mmol of oleylamine, and 1 mmol of $Fe(CO)_5$ were injected through a syringe. The reaction mixture was then heated to the boiling temperature of phenyl ether (~260 °C) and refluxed for 30 min. after which it was cooled to room temperature.

The superhydride method retains the basic experimental setup used for the iron pentacarbonyl method. However, unlike the iron pentacarbonyl method (which involves the thermal decomposition of $Fe(CO)_5$ added at 100 °C), the superhydride synthesis uses 0.5 mmol of $FeCl_2$ along with $Pt(acac)_2$, 1,2 hexadecanediol, and diphenyl ether at room temperature. The reaction mixture was first heated to 100 °C and then 0.5 mmol of oleic acid and 0.5 mmol of oleylamine were injected through a syringe. The reactants were then heated to 200 °C and 2.5 ml of superhydride ($LiBEt_3H$) was injected into the reaction mixture to reduce the $FeCl_2$. After refluxing the reaction mixture for 30 min. at the boiling temperature of the solvent, it was cooled to room temperature.

The mechanism of formation of FePt nanoparticles by the pentacarbonyl synthesis has been previously reported.[12] To investigate the mechanism of formation of the FePt nanoparticles by the superhydride method, 1 ml of the dispersion was extracted and quenched in 7 ml of ethanol (to bring the dispersion to room temperature) at three different stages of the reaction (a) stage one, at 200 °C just before the addition of superhydride; (b) stage two, at 260 °C after the addition of superhydride; and (c) stage three, at 260 °C after 30 min. of refluxing. The reaction mixture was further refluxed for extended periods of time and specimens were extracted after 90 and 150 min.

The extracted reaction mixtures contained FePt nanoparticles along with various reaction by-products. For this study, it was essential to separate the particles from by-products and surfactants, the presence of which causes charging effects under the electron beam in the scanning transmission electron microscopy-energy dispersive spectroscopy (STEM-EDS) analysis. The particles were washed by allowing the dispersion from the final reaction mixture to precipitate in an ethanol solution. The supernatant was drained and the particles settled at the bottom of the flask were centrifuged at 3000 rpm for 10 min. A mixture of hexane and 0.5 vol % oleic acid and oleyl amine was added to redisperse the particles. This specimen was then centrifuged again. The dark colored FePt nanoparticle dispersion that did not settle at the bottom of the vial was dropped in ethanol, which allowed the particles to precipitate. The specimen was again centrifuged to precipitate the particles and the supernatant was discarded. The resulting clean particles were then redispersed in hexane.

X-ray diffraction (XRD) measurements were carried out using a Rigaku 1-D/ MAX-2BX diffractometer operating at 40 kV and 40 mA with a Cu K_α radiation source to determine the crystal structure of the particles. The XRD specimens were prepared by drop drying the nanoparticle dispersion on a Si wafer. The average composition of the nanoparticle dispersion was measured using EDS on a Phillips XL-30 scanning electron microscope (SEM) operating at 20 kV. Bright-field images were acquired and single particle composition measurements were performed using a 200 keV field emission FEI Tecnai F20 supertwin (scanning) transmission electron microscope (TEM). The TEM specimens were prepared by drop drying a highly dilute dispersion of the clean nanoparticles onto a 50 nm thick silicon nitride supporting window. The EDS measurements were carried out in a *Z*-contrast imaging mode using a high angle annular dark-field detector in STEM. Cross-correlation drift correction was performed during the single particle EDS measurements, with time intervals typically of 10 s. Normal acquisition times were 200 s. The STEM operated with a FEI spot-size designation of 6 to produce adequate x-ray fluorescence counts, with a typical EDS spatial resolution of ~1–2 nm. Background subtracted integrated intensity of the peaks corresponding to Fe-*K* and Pt-*L* lines in the EDS spectrum were used for the quantification using the Tecnai Imaging and Analysis software. A homogeneous FePt thin film whose composition was verified by Rutherford Backscattering was used to qualify the Cliff-Lorimer factors for the EDS quantification. Care was taken during the experiments to analyze only those particles that were well separated (>25 nm) from any other single particle or a group of particles to remove any potentially unwanted EDS signals from neighboring particles. It should be noted that a Cl-*K* peak was observed in the spectrum. This peak was found to be a residual artifact of the manufacturing

process of the silicon nitride supporting window. It is critical that this peak in the EDS spectrum be accounted for since the particles are synthesized from $FeCl_2$.

III. FEP CALCULATIONS FROM MONTE CARLO SIMULATIONS

FEP calculations via Monte Carlo simulations were performed to study the thermodynamic driving forces for the movement of Fe atoms from the surface to the core of a Pt cluster. Additionally, the thermodynamic driving force for the movement of Fe atoms from the surface to a layer beneath the surface of FePt nanoparticles of varying composition was studied. The minimum in the free energy corresponds to the most thermodynamically stable configuration among the structures explored (in the absence of kinetic limitations). The gradient in the free energy is proportional to the thermodynamic driving force between the current configuration and neighboring configurations. Thus, as the gradient approaches zero, the likelihood of a structural transition decreases. A 2 nm model nanoparticle was constructed for the first part of the investigation, with Pt atoms occupying a fcc lattice with a lattice parameter of 0.392 nm.[11] Initially a Pt nanoparticle model was constructed where upon 100 Pt atoms on the surface were randomly selected and replaced with Fe atoms, so that Fe atoms were randomly distributed over the surface of the Pt cluster. FEP via Monte Carlo simulations was then performed in the canonical ensemble, where the potential energy of the system, arising from the metal–metal interactions, was calculated using the embedded atom method potential developed by Wadley *et al.*[13] This potential has been shown to predict the physical properties and binding energies of alloys reasonably accurately.[13,14]

The simulation was executed by allowing the system to equilibrate for 10^7 Monte Carlo steps at a temperature of 373 K. Once equilibration was complete, the accumulated free energy difference for exchanging an Fe atom between layers, at periodic intervals of 1000 steps for a total of 2×10^7 steps was calculated using a forward sampling scheme. At the start of the simulation, one Fe atom from the surface (layer 0) was identified and singled out for the free energy investigation. The FEP sampling was carried out by exchanging the marked Fe atom with a Pt atom in the layer immediately beneath the surface (layer 1). To implement this, a Pt atom from the structure was selected at random and the distance of the chosen Pt atom from the initially marked Fe atom was calculated. If the distance between the two atoms was greater than a cutoff distance (the layer to layer separation), the switch was rejected and the search repeated until the desired cutoff criterion was met. In order to calculate the free energy change of the switch, the potential energy of the system was calculated before and after the switching procedure. The potential energy difference was then recorded for statistical accumulation and for the calculation of ensemble averages. The free energy change at each step is calculated according to[15]

$$\Delta A = -k_B T \ln[\langle \exp(-\beta \Delta V)\rangle_0], \quad (1)$$

where ΔA is the free energy change, ΔV is the change in the potential energy of the system because of the switching, k_B is the Boltzmann constant, T is the temperature, β is $(k_B T)^{-1}$, and $\langle\ \rangle_0$ is the ensemble average taken in the reference system.

Once the simulation was complete, the average free energy difference from all the switches during the course of the simulation was recorded as the net free energy change for the motion of an Fe atom from the surface (layer 0) to the layer immediately beneath it (layer 1). This simulation procedure was repeated five times (with the same Fe atom initially chosen for investigation) in order to generate statistical averages. At the completion of this first step, the Fe atom initially marked for investigation was exchanged with a Pt atom occupying the layer immediately beneath the surface, which generated a new structural model, with the Fe atom now occupying a position in layer 1. The procedure was repeated in a stepwise fashion until the Fe atom reached the fourth layer in the structure, which is approximately the central layer in the nanoparticle (the 2 nm particle model contains eight layers from side to side). The simulations were executed until a total of ten Fe atoms had been moved from the surface to the core of the particle and subsequently with 16 and then 24 Fe atoms occupying the core.

In the second part of the study, the free energy change for the movement of an Fe atom from the surface (layer 0) to a layer immediately beneath the surface (layer 1), for 2 nm $A1$ FePt nanoparticle models, was investigated for compositions varying from 35 at. % Fe to 70 at. % Fe. The simulation procedure for this study was the same as that discussed earlier.

IV. RESULTS

FePt nanoparticles were synthesized by two different procedures, iron pentacarbonyl and superhydride, as described earlier in Sec. II. Both processes produced metastable nanoparticles with the $A1$ structure. TEM bright-field images of the FePt nanoparticles from each process are shown in Figs. 1(a) and 1(b), respectively. We observed the average size of these particles, as determined by TEM, to be 2.80 ± 0.38 nm and 2.90 ± 0.72 nm for particles synthesized by the superhydride and iron pentacarbonyl methods, respectively.

The average composition, measured by SEM-EDS, was determined to be $Fe_{58}Pt_{42}$ for the iron pentacarbonyl synthesis and $Fe_{45}Pt_{55}$ for the superhydride synthesis. The individual particle-to-particle composition distributions for particles synthesized from the iron pentacarbonyl and superhydride methods are shown in Figs. 2(a) and 2(b), respectively. The range in composition for the particles that were refluxed at 260 °C for 30 min was large for the iron pentacarbonyl synthesis (10 at. % Pt to 100 at. % Pt, with a standard deviation, σ, equal to 21) whereas the superhydride synthesis produced particles with less variation in composition (30 at. % Pt to 70 at. % Pt, with $\sigma=9.3$) with a large percentage of particles having a composition close to the average value.

X-ray diffraction peaks from the stage-wise analysis of the superhydride synthesis are shown in Fig. 3 and show a shift in the {111} peak to a higher 2θ angle, with a corre-

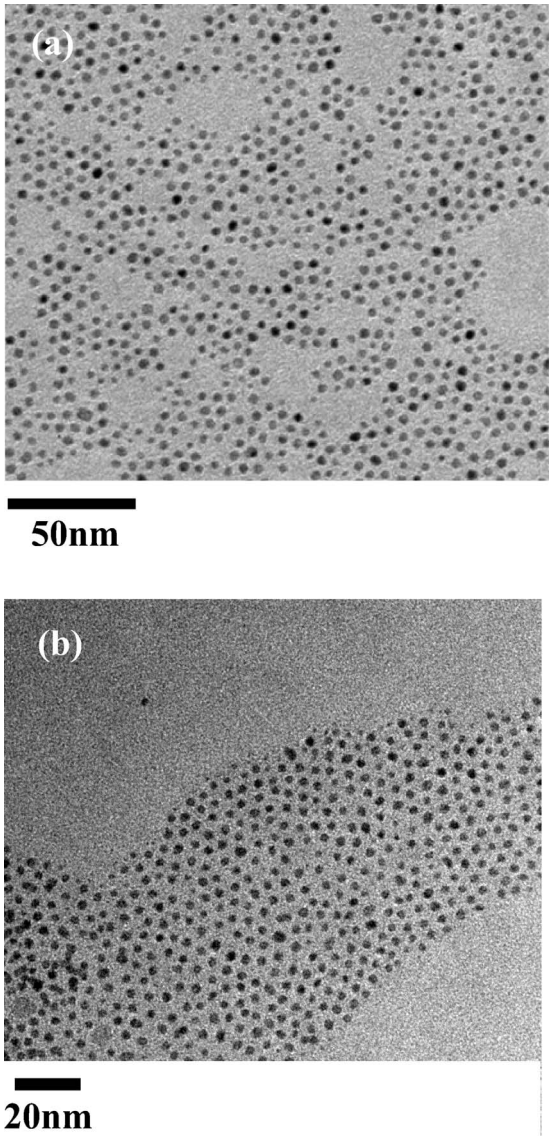

FIG. 1. Bright-field TEM images for particles synthesized by (a) iron pentacarbonyl and (b) superhydride.

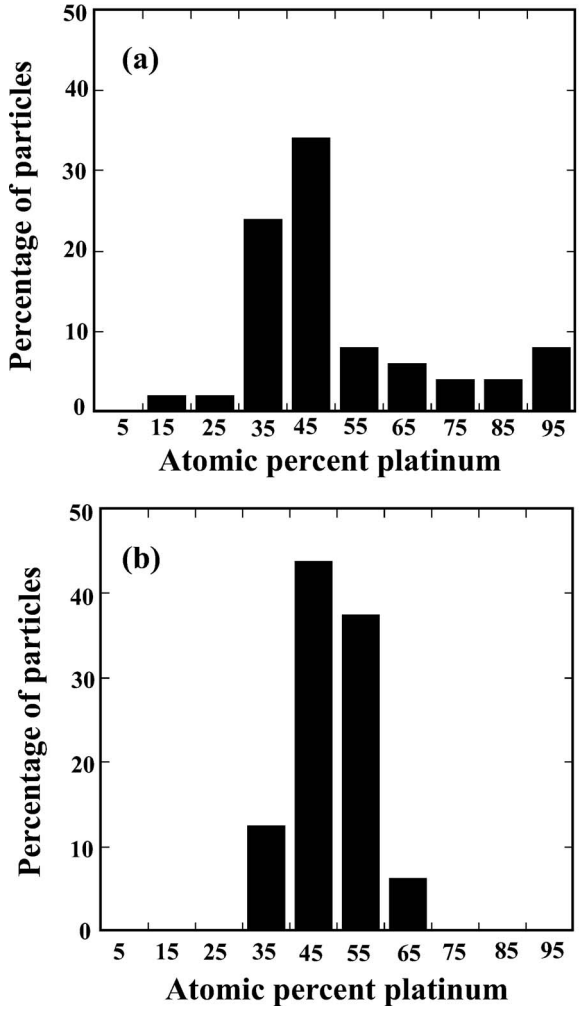

FIG. 2. Particle-to-particle composition distribution for FePt nanoparticle dispersion synthesized by (a) iron pentacarbonyl and (b) superhydride. The distribution in the composition of the particles for the superhydride process is narrower than the iron-pentacarbonyl process. Forty-seven and fifty individual nanoparticles were analyzed for the iron pentacarbonyl and superhydride histograms respectively.

sponding decrease in the d spacing of the {111} plane from 0.2266 to 0.2250 nm. Single particle STEM-EDS analysis was performed for particles from all three stages of the synthesis. The composition distributions for stages one, two, and three are shown in Figs. 4(a)–4(c), respectively. The distributions distinctly shift from being Pt rich in Fig. 4(a) to being around the final average value for the composition in Fig. 4(c).

Additional STEM-EDS was performed on particles extracted from the reaction mixture after 90 and 150 min of refluxing and the composition distributions for the respective dispersions are shown in Figs. 5(a) and 5(b). The particle-to-particle compositional variation continued to narrow with reflux time, but there was no change in the average composition of the particles.

FEP calculations were used to determine the free energies associated with Fe migrating from the surface of a Pt cluster into the subsurface and core. This mechanism is consistent with experimental observations showing the initial formation of Pt-rich clusters into which Fe is incorporated. The cumulative change in the free energy of the system, when an Fe atom on the surface (layer 0) moves into the cluster, as a function of the layer-by-layer position of the Fe atom in the structure is shown in Figs. 6(a)–6(c). The cumulative free energy change for the movement of an Fe atom from the surface (layer 0) to the core (layer 4) of the particle as a function of the number of Fe atoms in the initial core is shown in Fig. 7. Steps with negative slopes in Figs. 6(a)–6(c) indicate a favorable net thermodynamic driving force for each movement. The following can be inferred from the nature of this plot (i) the very first Fe atom that moves results in a net negative free energy change of −2.54 eV by the time it reaches the fourth layer in the structure, which is approximately at the center of the cluster, (ii) the magnitude of the thermodynamic driving force is large for movement from the surface into the very first layer, but becomes progressively smaller as the Fe atom moves further into the particle, (iii) the flatness of the curve in the last region of movement indicates that the driving force for that event is fairly low, (iv) movement of subsequent Fe atoms from the surface results in free energy changes that oscillate around those of the first Fe

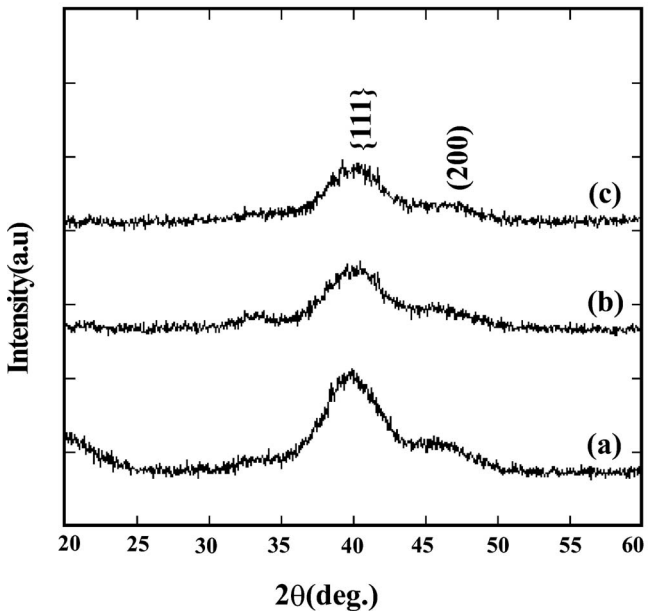

FIG. 3. XRD curves of FePt nanoparticles extracted at different stages in the superhydride synthesis process (a) stage one, (b) stage two, and (c) stage three. A slight shift in the 2θ position of the {111} reflection indicates the addition of Fe atoms in the nanoparticles as the synthesis progresses.

atom until about 4 to 5 Fe atoms have moved into the cluster, (v) as the number of Fe atoms in the core region of the cluster increases, the thermodynamic driving force for movement of Fe further into the subsurface gradually decreases as shown in Fig. 7.

To study the relationship between the composition of a nanoparticle and the thermodynamic driving force for the initial incorporation of Fe from the surface, FEP simulations were performed with FePt nanoparticle models ranging in composition from 35 to 70 at. % Fe as shown in Fig. 8. The FEP shows a free energy change of −0.094 eV for the motion of an Fe atom from the surface (layer 0) to a layer immediately beneath the surface (layer 1) for a nanoparticle with a composition of 35 at. % Fe and the value increases to 0.334 eV for a particle with a 70 at. % Fe composition. A steady decrease in the thermodynamic driving force for movement occurs with increasing Fe content in the particle, as shown in the plot of the free energy change versus composition in Fig. 8.

V. DISCUSSION

The composition distributions shown in Figs. 2(a) and 2(b) suggest that the superhydride method of making FePt nanoparticles is better suited for the synthesis of particles with a relatively higher uniformity in particle-to-particle composition distribution. Based on the results of the stage-wise study of the superhydride reaction process, we conclude that the dominating mechanism in the formation of the FePt nanoparticles is one in which Pt rich seed clusters initially form and the subsequent reduction of Fe results the incorporation of Fe atoms within these seed clusters.

The shift in the d spacing in our XRD studies of the three different stages of the superhydride reaction process

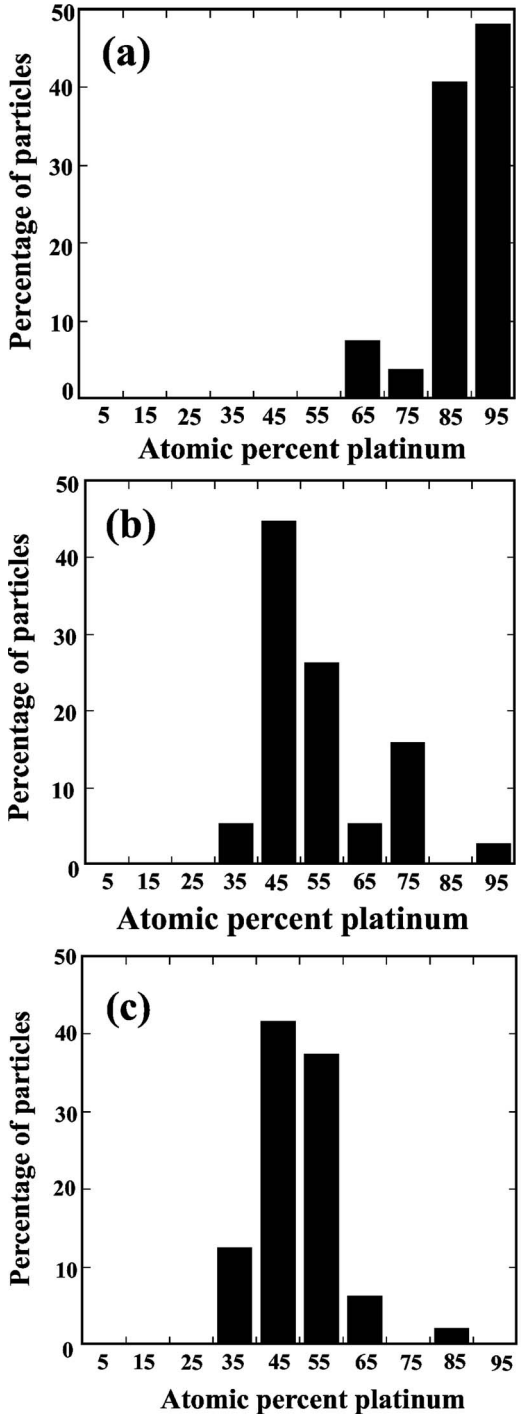

FIG. 4. Single particle composition distribution for different stages of the superhydride synthesis process (a) stage one (before the addition of superhydride at 200 °C), (b) stage two (at 260 °C), and (c) stage three (after 30 min. refluxing at 260 °C). Thirty-four, forty, and fifty individual particles were analyzed for stage one, stage two, and stage three, respectively.

provide an indication that Fe was incorporated into the nanoparticles as the synthesis progressed.[9] The STEM-EDS studies on the three stages of the reaction showed the presence of large percentages of Pt rich particles in stage one and the absence of any Fe rich particles. This indicates that at this stage of the synthesis the reaction mixture is composed of Pt rich clusters and mostly unreduced $FeCl_2$. These Pt rich clusters are obtained from the reduction of $Pt(acac)_2$ by 1,2

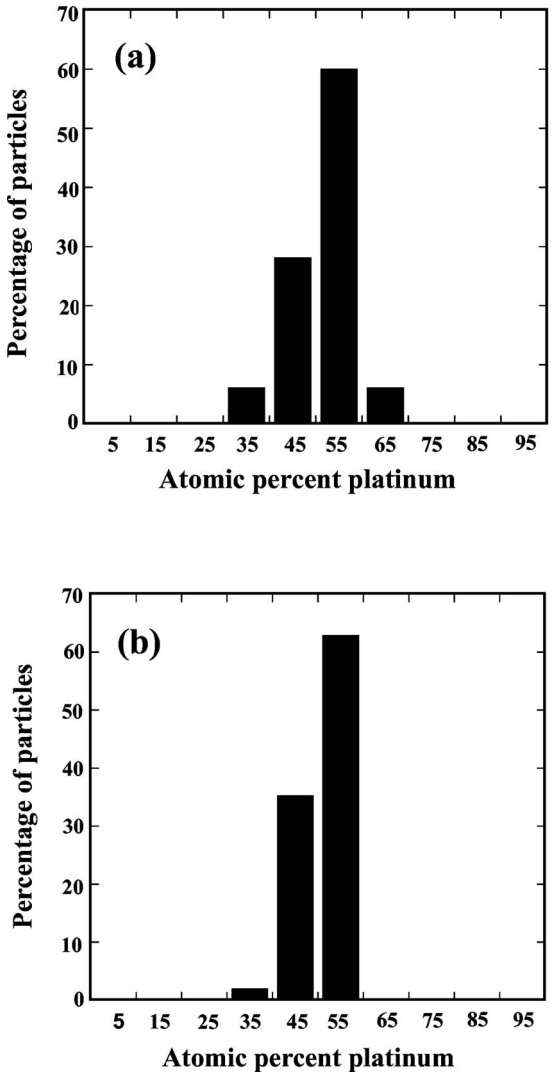

FIG. 5. Distribution in composition for nanoparticle dispersion refluxed at 260 °C for (a) 90 and (b) 150 min. The distribution in composition narrows with reflux time. Fifty individual particles were analyzed for both the 90 and 150 minutes reflux time dispersion.

hexadecanediol.[1] The composition distributions corresponding to stages two and three of the reaction show a shift toward the average value of $Fe_{45}Pt_{55}$.

One aspect of this mechanism is that Fe atoms must nucleate on the surface of the Pt rich seed clusters and then move into the clusters. The FEP simulations indicate that the movement of Fe into the cluster is indeed thermodynamically favorable. However, it must be stressed that these simulations do not provide any information about the incorporation kinetics, which may mask the equilibrium thermodynamics that are predicted here. The results of the FEP simulations suggest that Fe atoms thermodynamically favor being in a position somewhere within the cluster as opposed to staying on the surface. It is important to note the different regions or layers of movement in Figs. 6(a)–6(c). Movement into the very first layer beneath the surface of the cluster shows a fairly large favorable free energy change even for the movement of the 25th Fe atom [Fig. 6(c)]. As the number of Fe atoms in the core region increases, the cluster prefers to accommodate Fe atoms elsewhere in the

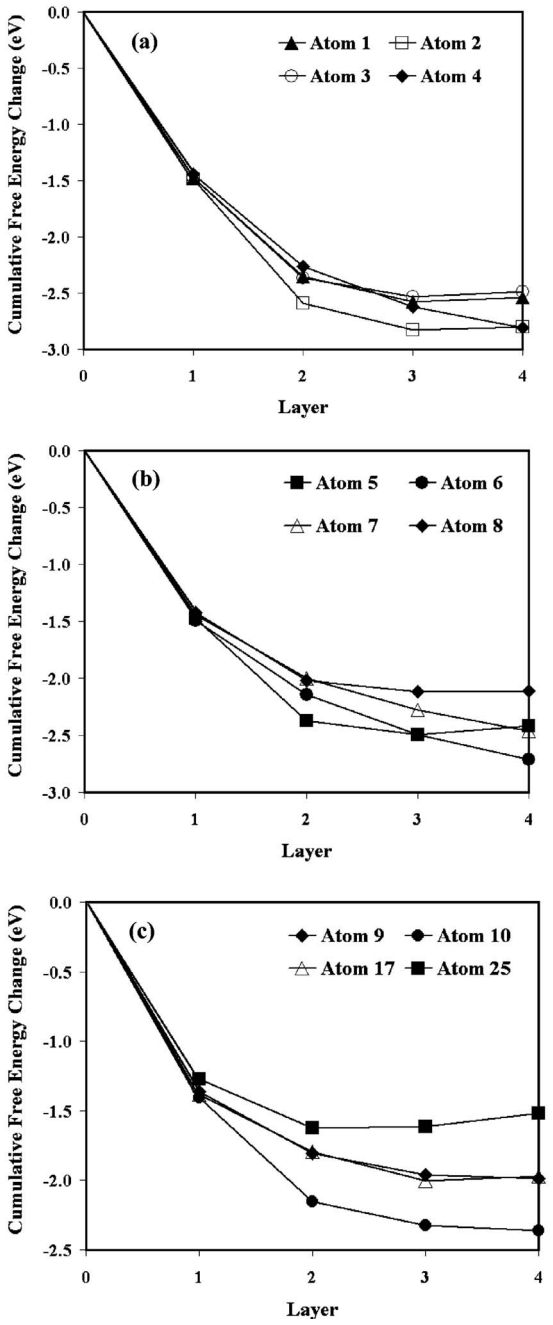

FIG. 6. Simulation predictions of the cumulative change in free energy for an Fe atom moving from the surface into subsequent layers of a 2 nm Pt nanoparticle. The free energy change increases with increasing Fe concentration in the core. Layer 0 represents the surface and layer 4 represents the core. (a) and (b) show the free energy change for atoms 1–4 and 5–8, respectively. (c) shows the free energy change for atoms 9, 10, 17, and 25.

structure where the concentration of Fe is less. The positive slope for the movement of the 25th Fe atom into layers 3 and 4 indicates that this movement is unfavorable, which suggests that the core has reached a thermodynamic limit for Fe concentration.

The FEP also predicts an equilibrium composition of ~43 at. % Fe for the movement of Fe into the subsurface for 2 nm particles. Moreover, the FEP calculations show that Fe prefers to be accommodated in the subsurface. The experimental data, for particles with similar sizes to the models used in the FEP, show that a majority of the particles synthe-

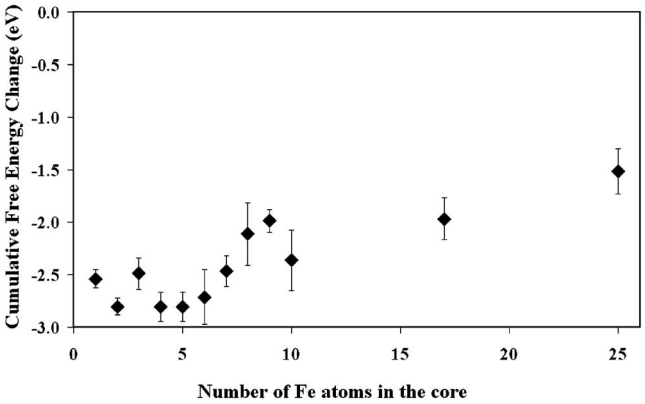

FIG. 7. Predictions of the cumulative free energy change vs. the number of Fe atoms in the initial core of a 2 nm Pt-rich nanoparticle.

sized by the superhydride method have a composition of ~45 at. % Fe. If the dominating mechanism in the formation of these nanoparticles is the formation of a Pt seed cluster which then absorbs Fe atoms from the surface of the cluster, regardless of the kinetic limitations, there exists a thermodynamic limit for the capacity of Fe sub-surface incorporation. This tendency could provide a self-limiting control for Fe incorporation into the Pt seeds. This indicates that, the superhydride method, which produces a much narrower composition distribution, is more successful than the pentacarbonyl precursor method in facilitating said mechanism.

There are few reports in the literature about the effect of refluxing time on the quality of the nanoparticle dispersion. It is possible that 30 min. of reflux time is not sufficient to produce a final composition distribution that approaches equilibrium. The results on the composition distribution after extended refluxing show that, although the composition not does show any change in the average value, it does narrow further toward the apparent thermodynamic equilibrium predicted by the FEP simulations.

The difference in the composition distribution in the iron pentacarbonyl and superhydride methods can be attributed primarily to the difference in the reduction process of the Fe precursor. The iron pentacarbonyl process involves the thermal decomposition of $Fe(CO)_5$ at a temperature of ~130 °C, which means that the decomposition of Fe and the reduction of Pt in this process occurs almost simultaneously. The highly volatile nature of $Fe(CO)_5$ (boiling temperature 103 °C) may contribute to a slow and inhomogenous decomposition process. It is possible that this interferes with the formation of a homogeneous set of Pt seed clusters, leading to a wider distribution of composition in the final product. The superhydride process involves a more instantaneous reduction of the Fe precursor at a temperature of 200 °C, which is well above the temperature at which the Pt precursor is reduced. Therefore, the time interval between the reduction of the Fe and the Pt precursors probably facilitates a more homogenous formation of the Pt seed clusters and a uniform availability of Fe for incorporation into the Pt seeds. Thus, the Fe atoms heterogeneously nucleate and grow on the existing Pt seed clusters producing a dispersion that has a relatively narrow distribution in composition once the thermodynamic equilibrium concentration is achieved.

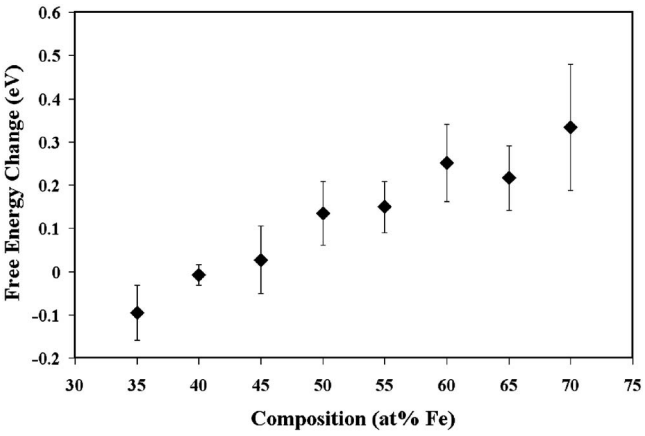

FIG. 8. Predictions of the free energy change vs. composition (% Fe) of a nanoparticle (random fcc structure) for the movement of an Fe atom from the surface (layer 0) to a layer just beneath it (layer 1).

VI. SUMMARY

In the present study, the mechanism of formation of FePt nanoparticles synthesized by the superhydride method has been analyzed. The dominating mechanism in the formation of these nanoparticles involves the formation of a Pt rich seed cluster, on which Fe atoms nucleate and then move into the cluster. The iron pentacarbonyl route produces particles that have a markedly wider composition distribution ranging from 10 to 100 at. % Pt, than particles produced by the superhydride method which are within 30 to 70 at. % Pt. The FEP calculations predict that there is a thermodynamic limit on the composition of ~43 at. % Fe for a 2 nm FePt cluster; a majority of the ~2 nm particles synthesized by the superhydride method have a composition of ~45 at. % Fe which is in close agreement to the composition limit predicted by the FEP. The difference in the range of the composition distribution between the two synthesis methods is attributed to the differences in the dynamics of the decomposition and reduction of the Fe precursor in the two methods.

ACKNOWLEDGMENTS

The authors gratefully acknowledge the National Science Foundation Materials Research Science and Engineering Center (DMR-0213985) and the Federal Transit Administration (Award No. AL-26-7024-00) for supporting this work. The Tecnai TEM was acquired through the National Science Foundation Major Instrumentation Program (DMR-0421376). Simulations were performed on the NRAC/TeraGrid and the Alabama Supercomputing Authority. Dr. David E. Nikles and Dr. J. W. Harrell are thanked for helpful comments.

[1] S. Sun, C. B. Murray, D. Weller, L. Folks, and A. Moser, Science **287**, 1989 (2000).
[2] D. Weller, A. Moser, L. Folks, M. E. Best, W. Lee, M. F. Toney, M. Schwickert, J.-U. Thiele, and M. F. Doerner, IEEE Trans. Magn. **36**, 10 (2000).
[3] Z. R. Dai, S. Sun, and Z. L. Wang, Nano Lett. **1**, 443 (2001).
[4] S. Kang, Z. Jia, S. Shi, D. E. Nikles, and J. W. Harrell, Appl. Phys. Lett. **86**, 062503 (2005).
[5] S. Kang, Z. Jia, S. Shi, D. E. Nikles, and J. W. Harrell, J. Appl. Phys. **97**,

10J318 (2005).
[6]K. Elkins, D. Li, N. Poudyal, V. Nandwana, Z. Jin, K. Chen, and J. P. Liu, J. Phys. D **38**, 2306 (2005).
[7]M. Chen, J. P. Liu, and S. Sun, J. Am. Chem. Soc. **126**, 8394 (2004).
[8]S. Sun, S. Anders, T. Thomson, J. E. E. Baglin, M. F. Toney, H. F. Hamann, C. B. Murray, and B. D. Terris, J. Phys. Chem. B **107**, 5419 (2003).
[9]S. Sun and H. Zeng, J. Am. Chem. Soc. **124**, 8204 (2002).
[10]A. C. C. Yu, M. Mizuno, Y. Sasaki, and H. Kondo, Appl. Phys. Lett. **85**, 6242 (2004).
[11]T. J. Klemmer, N. Shukla, C. Liu, X. W. Wu, E. B. Svedberg, O. Mryasov, R. W. Chantrell, and D. Weller, Appl. Phys. Lett. **81**, 2220 (2002).
[12]H. G. Bagaria, D. T. Johnson, C. Srivastava, G. B. Thompson, M. Shamsuzzoha, and D. E. Nikles, J. Appl. Phys. **101**, 104313 (2007).
[13]H. N. G. Wadley, X. Zhou, R. A. Johnson, and M. Neurock, Prog. Mater. Sci. **46**, 329 (2001).
[14]X. W. Zhou, H. N. G. Wadley, R. A. Johnson, D. J. Larson, N. Tabat, A. Cerezo, A. K. Petford-Long, G. D. W. Smith, P. H. Clifton, R. L. Martens, and T. F. Kelley, Acta Mater. **49**, 4005 (2001).
[15]M. P. Allen and D. J. Tildesley, *Computer Simulation of Liquids* (Oxford, New York, 1987).